Unusual NMR, EPR, and Mössbauer Properties of *Chromatium vinosum* 2[4Fe-4S] Ferredoxin†

Panayotis Kyritsis,‡ Rainer Kümmerle,§ J. Gaspard Huber,§ Jacques Gaillard,§ Bruno Guigliarelli,|| Codrina Popescu,⊥ Eckard Münck,⊥ and Jean-Marc Moulis*,‡

Département de Biologie Moléculaire et Structurale, Laboratoire Métalloprotéines, CEA, 17 rue des Martyrs, 38054 Grenoble Cedex 9, France, Département de Recherche Fondamentale sur la Matière Condensée, SCIB/SCPM, CEA, 17 rue des Martyrs, 38054 Grenoble Cedex 9, France, Laboratoire de Bioénergétique et Ingénierie des Protéines, UPR 9036 CNRS, 31 Chemin Joseph Aiguier, 13402 Marseille Cedex 20, France, and Department of Chemistry, Carnegie Mellon University, Pittsburgh, Pennsylvania 15213

Received December 8, 1998; Revised Manuscript Received February 17, 1999

ABSTRACT: The ferredoxin from *Chromatium vinosum* (CvFd) exhibits sequence and structure peculiarities. Its two $Fe_4S_4(SCys)_4$ clusters have unusually low potential transitions that have been unambiguously assigned here through NMR, EPR, and Mössbauer spectroscopy in combination with site-directed mutagenesis. The $[4Fe\text{-}4S]^{2+/1+}$ cluster (cluster II) whose coordination sphere includes a two-turn loop between cysteines 40 and 49 was reduced by dithionite with an $E^{\circ\prime}$ of −460 mV. Its $S = {}^1/_2$ EPR signal was fast relaxing and severely broadened by **g**-strain, and its Mössbauer spectra were broad and unresolved. These spectroscopic features were sensitive to small perturbations of the coordination environment, and they were associated with the particular structural elements of CvFd, including the two-turn loop between two ligands and the C-terminal α-helix. Bulk reduction of cluster I ($E^{\circ\prime} = -660$ mV) was not possible for spectroscopic studies, but the full reduction of the protein was achieved by replacing valine 13 with glycine due to an ≈60 mV positive shift of the potential. At low temperatures, the EPR spectrum of the fully reduced protein was typical of two interacting $S = {}^1/_2$ $[4Fe\text{-}4S]^{1+}$ centers, but because the electronic relaxation of cluster I is much slower than that of cluster II, the resolved signal of cluster I was observed at temperatures above 20 K. Contact-shifted NMR resonances of β-CH_2 protons were detected in all combinations of redox states. These results establish that electron transfer reactions involving CvFd are quantitatively different from similar reactions in isopotential 2[4Fe-4S] ferredoxins. However, the reduced clusters of CvFd have electronic distributions that are similar to those of clusters coordinated by the $Cys^{I}xxCys^{II}xxCys^{III}\cdots Cys^{IV}P$ sequence motif found in other ferredoxins with different biochemical properties. In all these cases, the electron added to the oxidized clusters is mainly accommodated in the pair of iron ions coordinated by Cys^{II} and Cys^{IV}.

[4Fe-4S] clusters are used as prosthetic groups in many biological systems, where they serve diverse functions, such as electron transfer, catalysis, oxygen sensing, and regulation of the action of nucleic acids (*1*). Yet, at the level of resolution attained by X-ray crystallographic studies of proteins, all structures of [4Fe-4S] cores appear to be very similar (*2*), with the exception of mitochondrial aconitase for which the cysteinyl ligand of one iron atom is replaced by an oxygen donor (*3*). The function of [4Fe-4S] clusters depends on a complex set of interactions with their immediate environments, including the surrounding amino acids and the solvent. Thus, a complete characterization of such interactions is desirable for understanding the function of [4Fe-4S] clusters in a given biological environment.

Recently, a new class of ferredoxins that includes the ferredoxin from *Chromatium vinosum* (CvFd)[1] has been characterized (*4*) and found to exhibit a very low reduction potential, around −660 mV versus the NHE (*5*, *6*), for one of the two $[4Fe\text{-}4S]^{2+/1+}$ clusters. The exact function of CvFd has not been determined, and possible redox partners of the protein have not yet been identified. CvFd is probably not functionally equivalent to isopotential ferredoxins because it cannot substitute for them in reconstituted electron transfer chains (*7*).

† Supported in part by a grant from the Groupement de Recherche CNRS "Métalloprotéines et Analogues de Synthèse" (to J.-M.M., J.G., and B.G.) and by National Science Foundation Grant MCB-9406224 (to E.M.).

* To whom correspondence should be addressed: CEA/Grenoble, DBMS/MEP, 17 rue des Martyrs, 38054 Grenoble Cedex 9, France. Telephone: 33 476885623. Fax: 33 476885872. E-mail: jean-marc.moulis@cea.fr.

‡ Département de Biologie Moléculaire et Structurale, Laboratoire Métalloprotéines, CEA.

§ Département de Recherche Fondamentale sur la Matière Condensée, SCIB/SCPM, CEA.

|| UPR 9036 CNRS.

⊥ Carnegie Mellon University.

[1] Abbreviations: CvFd, *C. vinosum* ferredoxin; NHE, normal hydrogen electrode; TRIQUAT, 1′,1″-trimethylene-2′,2″-dipyridinium dibromide; DMTQ, 4′,4″-dimethyl-1′,1″-trimethylene-2′,2″-dipyridinium dibromide; TOCSY, total correlation spectroscopy; NOESY, two-dimensional nuclear Overhauser enhancement spectroscopy; EXSY, exchange spectroscopy.

10.1021/bi982894u CCC: $18.00
Published on Web 04/24/1999

In an effort to further expand on the initial studies of the [4Fe-4S] clusters of CvFd (*5*, *8*), NMR, EPR, and Mössbauer spectroscopic studies have been carried out. In view of the importance of the polypeptide chain in modulating the properties of the iron−sulfur clusters, site-directed mutagenesis has been largely used to modify the environment of the clusters. These studies unambiguously associate the unusually low potential (−660 mV) redox transition of CvFd with the cluster coordinated by the conventional CxxCxxC···CP sequence motif. They also reveal new spectroscopic features for the other cluster.

EXPERIMENTAL PROCEDURES

Preparation of Proteins. Recombinant CvFd and a series of molecular variants, including the previously unpublished C57S CvFd (Cys-57 is the single noncoordinating cysteine of the sequence), have been produced by described procedures (*5*). Uniformly ^{15}N-enriched recombinant CvFd was prepared by growing *Escherichia coli* cells in a minimal medium containing 0.2 g/L $(^{15}NH_4)_2SO_4$ (99.8%, Cisotec, Inc., Miamisburg, OH) as the sole nitrogen source.

Molecular variants of CvFd are straightforwardly designated X*n*Y CvFd for the single site change in which amino acid X at position *n* is replaced by Y. In variant Δ1 CvFd, the Ala-Gln dipeptide replaces the eight amino acids in the two-turn loop between Cys-40 and Cys-49. K74− CvFd is the 73-residue protein in which the codon for Lys-74 has been exchanged for a stop codon, hence shortening about half of the terminal α-helix. These two changes are combined in Δ1K74− CvFd. Y44C and K74E CvFd were designed to further probe the specific structural features of CvFd occurring around cluster II, for which Cys-18, Cys-37, Cys-40, and Cys-49 are the ligands. These changes are described in detail elsewhere (*5*). D12G, V13G, Y30F, and C57S CvFd display single amino acid substitutions around cluster I coordinated by Cys-8, Cys-11, Cys-14, and Cys-53 (Figure 1). Strictly anaerobic conditions were ensured throughout all biochemical and spectroscopic experiments by using an anaerobic chamber (Jacomex, Livry-Gargan, France) and by maintaining an oxygen concentration of less than 2 ppm.

NMR Spectroscopy. NMR spectra were recorded on a 500 MHz Unity Plus Varian spectrometer, and protein samples (0.5−2 mM) were prepared in 20 mM potassium phosphate buffer (pH 8.2) unless otherwise stated, according to procedures described previously (*9*). Reduction was carried out with a 10-fold excess of sodium dithionite, the reduction potential of which can be estimated at ca. −580 mV under these conditions (*10*), sometimes supplemented with metallic Zn and viologens (methyl viologen or DMTQ) at concentrations that were ca. 100 times lower than that of the protein. Conditions for NOESY and EXSY spectra were similar to those previously implemented (*8*), with short mixing times of 5−10 ms.

EPR Spectroscopy. Protein samples (0.1−0.5 mM) in 20 mM potassium phosphate buffer (pH 8.2) were reduced by a 10−30-fold excess of sodium dithionite standardized against a calibrated thionin solution; 5 μM methyl viologen ($E_1° = -445$ mV), TRIQUAT ($E_1° = -550$ mV), and DMTQ ($E_1° = -680$ mV) were sometimes used as mediators. Potentials were measured with a combined electrode (Radiometer XM850 ET). The absorption spectrum was concomitantly monitored inside the anaerobic chamber with a Hewlett-Packard 8453 spectrophotometer connected through fiber optics (*12*).

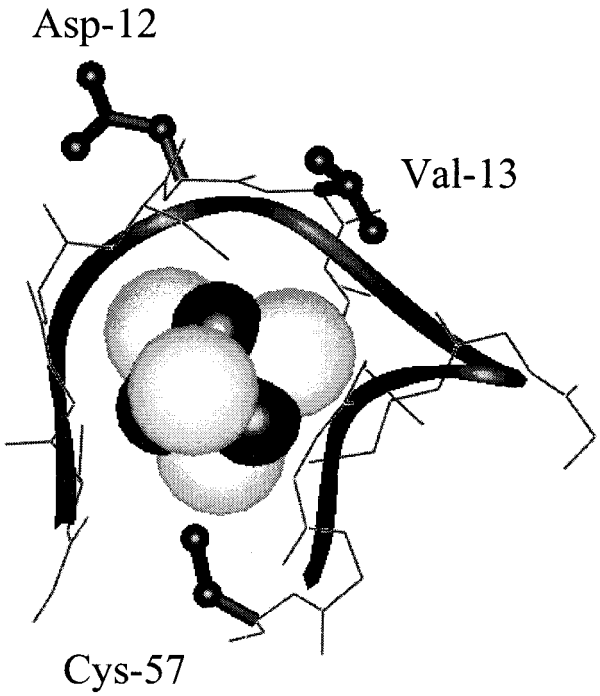

FIGURE 1: Schematic view of the peptide environment around cluster I of *C. vinosum* ferredoxin. A solid ribbon is drawn through the main chain of the model (*11*). The ball-and-stick representation is for amino acids discussed in the text and the space-filling representation for the cluster. Residues 12 and 13 are exposed to the solvent. Cluster II would be located at the bottom of the figure in the complete representation of the protein.

EPR spectra were recorded on a Bruker ESP 300E spectrometer operating at X-band (9 GHz) or Q-band (35 GHz), and equipped with an Oxford Instrument ESR 900 (X-band) or CF 935 (Q-band) helium flow cryostat. Numerical simulations of EPR spectra were based on a **g**-strain statistical procedure (*13*) in which the distribution of the **g**-tensor around a mean value $\mathbf{g_0}$ is described by a three-dimensional tensor **p**. The principal elements p_i of this tensor are random variables which are statistically correlated (correlation coefficients r_{ij}) and characterized by their standard deviations σ_i. The adjustment of the various parameters of the model was facilitated by using the previously developed regression program REGRES (*14*).

Mössbauer Spectroscopy. ^{57}Fe-enriched CvFd was prepared by removing the clusters of recombinant protein by trichloroacetic acid precipitation and by reconstitution in the presence of ^{57}Fe prepared by acid solubilization of the metal (*15*). Mössbauer spectra were recorded in the constant acceleration mode (*16*).

RESULTS

A low potential [4Fe-4S] cluster can access two redox levels with formal Fe_4S_4 charges of 2+ (oxidized) or 1+ (reduced). 2[4Fe-4S] CvFd will thus be designated *(rr)* when both clusters are reduced, *(oo)* for the fully oxidized protein, *(or)* for molecules in which only cluster II (coordinated by Cys-18, -37, -40, and -49) is reduced, and *(ro)* in which only cluster I (coordinated by Cys-8, -11, -14, and -53) is reduced.

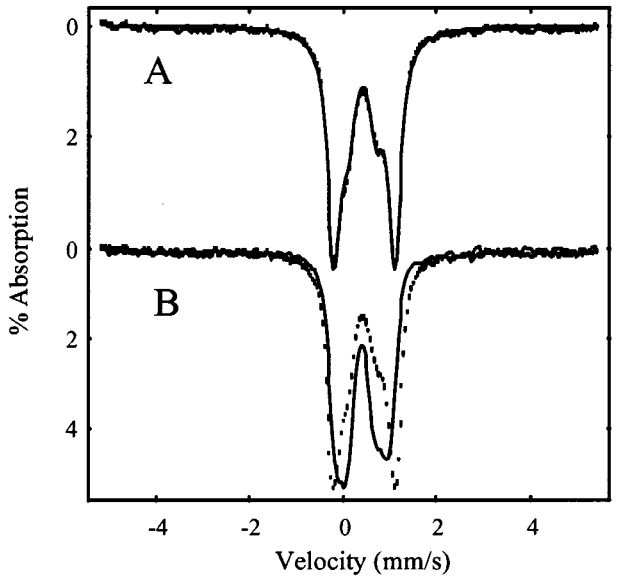

FIGURE 2: Mössbauer spectra of oxidized CvFd. The data were recorded in a 45 mT external field applied parallel to the incident γ-radiation at 4.2 K (A) and 150 K (solid line in panel B). The solid line in panel A is a least-squares fit of the data, assuming four iron sites with the following ΔE_Q (millimeters per second) and δ values (millimeters per second): 1.30 and 0.47, 1.32 and 0.42, 1.23 and 0.46, and 0.61 and 0.41, respectively. The dotted line in panel B is the 4.2 K spectrum superimposed on the 150 K data (solid line).

Characterization of the Oxidized Protein

Mössbauer Studies. Figure 2 shows Mössbauer spectra of oxidized CvFd recorded at 4.2 K (A) and 150 K (B, solid line). The average isomeric shift and the observed quadrupole splittings are typical for $[4Fe\text{-}4S]^{2+}$ clusters. The 4.2 K spectrum can be approximated by two quadrupole doublets with a 3:1 intensity ratio, namely, a majority species with a ΔE_Q of 1.3 mm/s and a minority species with a ΔE_Q of 0.6 mm/s. The solid line in Figure 2A is a least-squares fit obtained by assuming four quadrupole doublets with the parameters listed in the figure caption. However, because as many as eight iron sites contribute to this spectrum, other spectral decompositions are possible. The superposition of the 150 K spectrum on the 4.2 K spectrum (Figure 2B) shows that the quadrupole splittings are temperature-dependent, suggesting that low-lying excited states are thermally accessible at 150 K, as observed for other $[4Fe\text{-}4S]^{2+}$ ferredoxins (*17*).

NMR Studies. The low-field ^{1}H NMR spectra of oxidized CvFd and of selected derivatives obtained by site-directed mutagenesis are shown in Figure 3. For comparison, the spectrum of *Clostridium acidurici* Fd is also shown. The number of signals between 10 and 20 ppm, most of them arising from cysteinyl β-protons (*8*), is approximately constant in all these spectra, but a few resonances are shifted in some of them. This spectral region has been probed by NOESY and TOCSY experiments tailored for studying fast relaxing nuclear spins. The availability of such extensive data sets has enabled us to revisit the previously proposed assignments and to complement them with ^{15}N NMR ones (Supporting Information).

NMR Signals of the Cys-40 Side Chain. The hyperfine contribution to the chemical shifts of protons in paramagnetic proteins includes contact and dipolar terms. In the case of

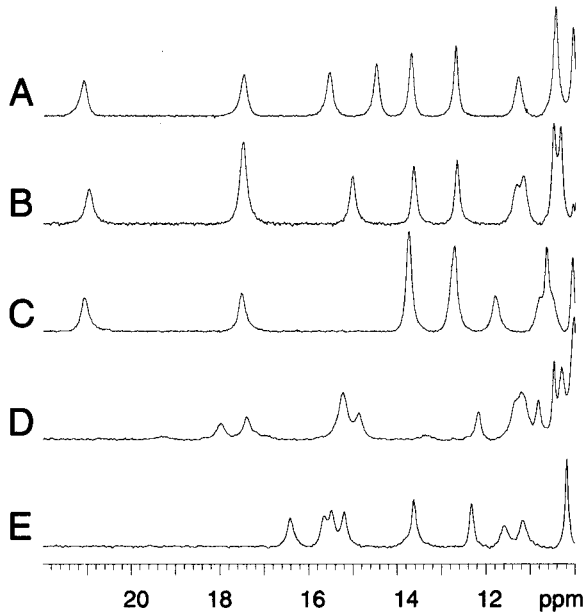

FIGURE 3: Low-field 500 MHz ^{1}H NMR spectra of oxidized 2[4Fe-4S] ferredoxins: (A) native, (B) D12G, (C) V13G, (D) Δ1 CvFd, and (E) *C. acidurici* Fd. The spectra were recorded at 298 K.

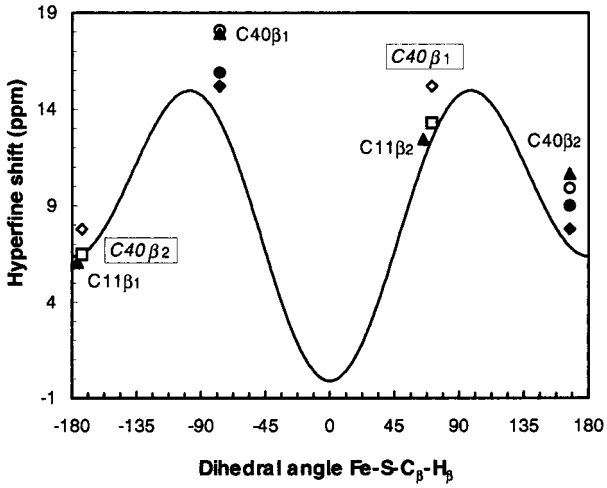

FIGURE 4: Contact shifts of cysteinyl protons in oxidized 2[4Fe-4S] ferredoxins. The hyperfine shifts, as defined in ref *8*, of the cysteinyl β-protons in *C. acidurici* Fd, including those of Cys-40 (□), were fitted (solid line) as a function of the dihedral angles obtained from the atomic resolution structure of the protein (*2*). The Cys-11 and Cys-40 protons of CvFd (▲) are labeled. The signals of the protons of Cys-40 in Y44C (○), Δ1K74− (●), and Δ1 (diamonds) are also plotted. In the latter case, the black diamonds correspond to the angle values of the native CvFd structure and the white ones (boxed and italicized labels) to those of the *C. acidurici* Fd structure.

β-protons of cysteine-coordinating $[4Fe\text{-}4S]^{2+}$ clusters, the dipolar contribution is usually weak. The contact term depends on the value of the dihedral angle formed by the Fe−S−C$_\beta$−H$_\beta$ bonds (resulting from orbital overlap involving the proton 1s orbital), and this dependence is described by a Karplus-type equation (*18*). The signals of Cys-40 β-protons in CvFd occur at 21.2 and 13.8 ppm and, as previously reported (*8*), lie somewhat outside the predicted dependence (Figure 4) calculated with the highest-resolution structure of *C. acidurici* Fd (*2*). The positions of these signals vary little for most CvFd variants studied here (less than 0.6 ppm for the most shifted signal), except for Δ1 and

Table 1: Comparison of Assignments for β-Cysteinyl Protons of Oxidized and Dithionite-Reduced CvFd with Those of *C. acidiruci* Fd[a]

	cluster I								cluster II							
	Cys-8		Cys-11		Cys-14		Cys-53		Cys-37		Cys-40		Cys-49		Cys-18	
	Hβ_1	Hβ_2	Hβ_1	Hβ_2	Hβ_1	Hβ_2	Hβ_1	Hβ_2	Hβ_1	Hβ_2	Hβ_1	Hβ_2	Hβ_1	Hβ_2	Hβ_1	Hβ_2
CvFd																
(or) δ (ppm)									35.9	51.0	60.8	38.1				73.0
(or) ΔT									C	C	AC	AC				AC
(oo) δ (ppm)	11.4	9.9[b]	9.0[b]	15.6	14.6	5.2[b]	9.1[b]	10.5	10.5	7.7[b]	21.2	13.8	17.6	4.0[b]	5.7[b]	12.8
C57S CvFd																
(or) δ (ppm)	11.4			15.0	14.6				36.1	51.2	60.5	37.8				73.2
(oo) δ (ppm)	11.3	10.0	8.9	15.0	14.6	5.1	8.5	10.7	10.5	7.9	21.2	13.8	17.5	4.2	6.9	12.8
	Cys-8		Cys-11		Cys-14		Cys-47		Cys-37		Cys-40		Cys-43		Cys-18	
	Hβ_1	Hβ_2	Hβ_1	Hβ_2	Hβ_1	Hβ_2	Hβ_1	Hβ_2	Hβ_1	Hβ_2	Hβ_1	Hβ_2	Hβ_1	Hβ_2	Hβ_1	Hβ_2
C. acidurici Fd[c]																
(oo) δ (ppm)	11.4	8.2	9.2	15.4	15.0	4.8	6.5	13.4	11.1	7.9	9.5	16.3	15.2	4.8	6.4	12.2

[a] Chemical shifts (δ) at 298 K, given for the oxidized *(oo)* and dithionite-reduced *(or)* proteins. ΔT indicates the dependence on temperature. C represents curie and AC anticurie. [b] Chemical shifts at 293 K. [c] Chemical shifts for *C. acidurici* Fd at 293 K and pH 7.8 were taken from ref *18*.

Δ1K74− CvFd, for which upfield shifts, of up to 3 ppm for the same signal, convert the pattern of hyperfine shifted signals into one more similar to that of *C. acidurici* Fd (Figure 3). These spectroscopic features suggest that the two variants of CvFd that lack the two-turn loop between cysteine residues 40 and 49 (*11*) are structurally closer to proteins exhibiting the conventional CxxCxxC···CP coordinating motif of [4Fe-4S] clusters.

The influence of the ring current of Tyr-44 at less than 5 Å from the Cys-40 β-protons to their chemical shifts has been estimated by a simple model (*19*) to be a negative fraction of 1 ppm. In agreement with this estimate, in Y44C CvFd the chemical shift of Hβ_2 Cys-40 decreases by the modest value of 0.7 ppm compared to that of CvFd and that of the less shifted Hβ_1 by an even smaller value (Figure 4). This shows, from both theoretical and experimental considerations, that the aromatic ring of Tyr-44 is only marginally responsible for the chemical shift discrepancies displayed by the signals of CvFd Cys-40 Hβ. The unexpectedly large values of the Hβ Cys-40 chemical shifts in CvFd may therefore originate from a slightly larger value of the spin density on the iron coordinated by this cysteine, perhaps as a result of the unusual conformation of this ligand (*11*).

NMR Signals of the Cys-11 Side Chain and Evidence for a pH Effect. The Cys-11 protons in D12G and V13G CvFd are close to the substituted amino acids (Figure 1), and their chemical shifts differ from those of CvFd (Figure 3 and Table 1). The plot of Figure 4 indicates that the chemical shift of Hβ_2 is expected to be more sensitive to a given angular variation of the Fe−S−C$_\beta$−H$_\beta$ dihedral angle than that of Hβ_1. The resonance of Cys-11 Hβ_2 in CvFd was also found to shift with pH; from the pH dependence of this signal, a pK_a of 6.3 was calculated (Figure 5). In contrast, the Cys-11 Hβ_2 proton of *C. acidurici* Fd, which resides in a similar structural environment (*2*, *11*), and that of D12G CvFd both exhibit pH-insensitive chemical shifts (Figure 5). The latter proteins lack the carboxylic group of Asp-12, and the combined data show that Cys-11 Hβ_2 senses the electrostatic potential contributed by this residue in CvFd.

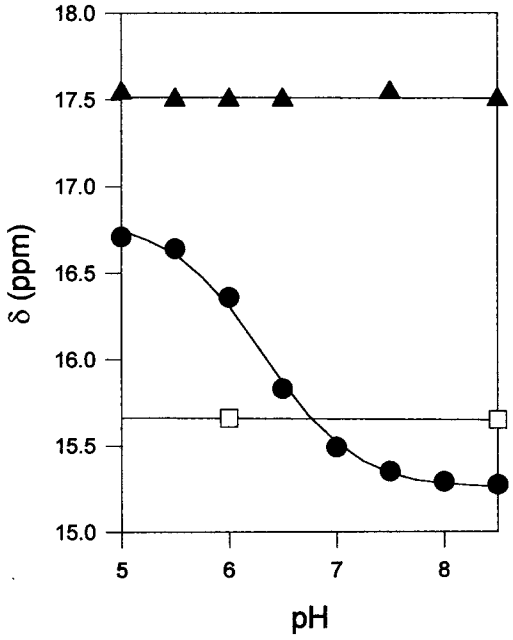

FIGURE 5: pH dependence of the Cys-11 Hβ_2 chemical shift. NMR spectra were recorded for *C. acidurici* Fd (□), D12G CvFd (▲), and CvFd (●). In the latter case, the curve is a fit of the experimental data with a pK_a value of 6.3.

One-Electron Reduction with Dithionite

EPR Studies. Dithionite-reduced CvFd has already been shown to display EPR spectra with unusual shapes (*8*). A similar X-band EPR spectrum recorded without interference from radicals is shown in Figure 6A. Compared to spectra of magnetically isolated $S = {}^1/_2$ [4Fe-4S]$^{1+}$ clusters, this rhombic spectrum had an unusual line shape with two major features at $g = 2.07$ and 1.89, broad wings at the high- and low-field ends, and an almost collapsed derivative-like feature at $g = 1.94$. This signal was also comparatively fast relaxing; for instance, at 10 K, saturation did not occur below 40 mW, and the signal disappeared by relaxation broadening at temperatures above 20 K. Below 20 K, no heterogeneous changes of the line shape were observed over a 0.01−200 mW range of microwave power, ruling out the possibility that more than one species contributes to the observed spectrum. No additional signals were detected in sweeps covering a 700 mT field range, indicating the absence of $S > {}^1/_2$ species. In addition, the same EPR features were observed for samples at different protein concentrations or at different ionic strengths or prepared during a reductive

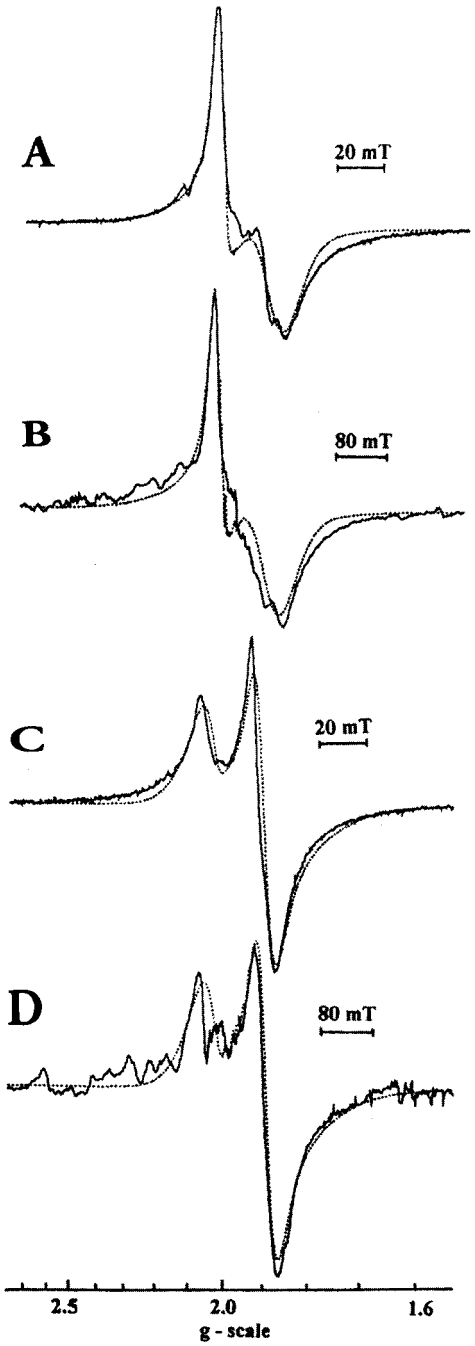

FIGURE 6: X-band and Q-band EPR spectra of dithionite-reduced CvFd: (A and B) CvFd and (C and D) Δ1 CvFd. Solid lines are experimental spectra recorded under the following conditions: temperature, 10 K; microwave frequency, 9.430 GHz (A and C) or 33.90 GHz (B and D); microwave power, 10 mW; and modulation amplitude, 1 mT (A and C) or 2 mT (B and D) at 100 kHz. Dotted lines are numerical simulations obtained with the following parameters: (A and B) $g_{X,Y,Z} = 1.894, 1.994, 2.096$, $\sigma_{X,Y,Z} = 0.043, 0.207, 0.0016$, Euler angles between tensors $\mathbf{g_0}$ and $\mathbf{p}$ of 23°, 43°, and −31°, correlation coefficients of 0.085, 0.935, and −0.264; (C and D) $g_{X,Y,Z} = 1.787, 1.890, 2.078$, $\sigma_{X,Y,Z} = 0.135, 0.027, 0.0027$, Euler angles between tensors $\mathbf{g_0}$ and $\mathbf{p}$ of −50°, 42°, and 30°, correlation coefficients of 1, 1, and 1.

titration of the protein with dithionite. The number of electrons transferred upon reducing the protein by dithionite is difficult to determine reliably because of the long time (ca. 30 min) that is required for attaining the equilibrium between these reactants (*5*). Nevertheless, using dithionite as the reductant, the spin concentration of several samples was found to be approximately 1 spin/CvFd, a smaller value than the one estimated previously (*8*). This observation suggests that only one cluster is reduced by dithionite, in agreement with the Mössbauer and NMR data presented below.

The same peculiar EPR line shape was also observed in the Q-band spectra (Figure 6B). The invariance of the spectral shape with the microwave frequency indicates the absence of magnetic coupling between two nearby [4Fe-4S]$^{1+}$ paramagnets. The similarity of the spectra of parts A and B of Figure 6 further indicates that the broadening of these EPR spectra is mainly due to **g**-strain. Usually, good simulations of EPR spectra arising from magnetically isolated [4Fe-4S]$^{1+}$ clusters in proteins can be obtained by a statistical description of **g**-strain (*13*) in which the mean tensor $\mathbf{g_0}$ and the fluctuation tensor **p** are colinear, the random variables p_i being positively fully correlated, i.e., $r_{ij} = 1$ (*20*−*23*). For dithionite-reduced CvFd, the best simulations obtained with such constraints correctly reproduced the central region of both the X-band and Q-band EPR spectra ($g_{X,Y,Z} = 1.89, 1.96, 2.065$; $\sigma_{X,Y,Z} = 0.03, 0.09, 0.016$), but not the broadening of the signal wings (not shown). Satisfactory simulations could only be achieved by rotating the **p** tensor with respect to $\mathbf{g_0}$ and by allowing partial correlations of random variables p_i (Figure 6A,B). Moreover, the standard deviations deduced from these simulations are significantly larger (especially σ_y) than those usually found ($5-15 \times 10^{-3}$) for $S = {}^1/_2$ [4Fe-4S]$^{1+}$ clusters (*21*−*23*).

The EPR spectra of most CvFd variants were quite similar (not shown); significant changes were only found for Δ1 (Figure 6C,D), K74E, and Δ1K74− CvFd (not shown), which display spectra more similar to those observed for typical protein-bound [4Fe-4S]$^{1+}$ clusters. For example, the X- and Q-band spectra of Δ1 CvFd have nearly axial shapes (Figure 6C,D), with fully developed peaks at $g = 2.07$ and 1.917, but they also display strongly broadened wings, like most of the CvFd variants. These EPR spectra were simulated as described above, with relatively large σ_i values, but fully correlated p_i variables ($r_{ij} = 1$) could be used (Figure 6C,D). The significance of these observations is discussed below.

Mössbauer Studies. The EPR results of Figure 6 have been complemented by Mössbauer spectroscopy of a ^{57}Fe-enriched CvFd sample. The 4.2 K Mössbauer spectrum of dithionite-reduced CvFd, shown in Figure 7A, consists of a superposition of a diamagnetic (see below) component exhibiting the same 3:1 quadrupolar pattern, like the spectrum of Figure 2A, and a paramagnetic component with broad, unresolved features. The two components are roughly in a 1:1 ratio, suggesting that one of the two clusters has been reduced by dithionite, while the other has remained oxidized. The paramagnetic species must be associated with the cluster that gives rise to the $S = {}^1/_2$ EPR signal of parts A and B of Figure 6. For comparison, Figure 7A also shows a theoretical spectrum that fits the well-resolved spectrum of the [4Fe-4S]$^{1+}$ ferredoxin from *Bacillus stearothermophilus*. The paramagnetic component of CvFd is much less resolved, suggesting that it is heterogeneously broadened, much like the **g**-strain-broadened EPR spectra (Figure 6).

In Figure 7B is shown an 8.0 T spectrum of dithionite-reduced CvFd. The solid line is a spectral simulation for a [4Fe-4S]$^{2+}$ cluster, assuming a diamagnetic ground state. The good match of the theoretical spectrum to the triplet structure

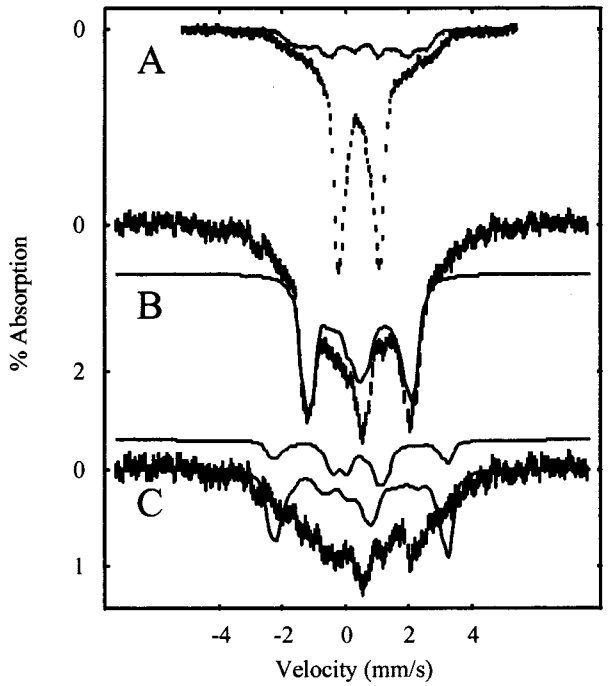

FIGURE 7: 4.2 K Mössbauer spectra of the dithionite-reduced CvFd recorded in (A) 45 mT and (B) 8.0 T fields. For comparison, the solid line in panel A is a theoretical spectrum obtained with the parameters that fit the reduced [4Fe-4S]$^{1+}$ cluster of *B. stearothermophilus* ferredoxin (*24*). The solid line through the data in panel B is a simulation for oxidized cluster I of CvFd, assuming that the cluster has a diamagnetic ground state (the parameters listed in the caption of Figure 2 were used). Spectrum C is the contribution of cluster II, obtained by subtracting the spectral simulation for the oxidized cluster I from the data in panel B. The solid line in panel C is a theoretical spectrum obtained with the parameters of the reduced [4Fe-4S]$^{1+}$ of *B. stearothermophilus* ferredoxin (*24*) [ΔE_Q (mm/s), δ (mm/s), η, $A_{X,Y,Z}$ (MHz)]: (1.32, 0.5, 0.78, −31.7, −32.5, −27.9), (1.89, 0.58, 0.32, 26.5, 13.5, 8.6). Above the data in panel C, the contribution of the ferrous pair of this cluster has been drawn for comparison.

of the data confirms this assumption. In Figure 7C is shown the 8.0 T spectrum of the paramagnetic component of this sample, obtained by subtracting the theoretical spectrum of the diamagnetic cluster (50%) from the data of Figure 7B. Conventional $S = {}^1/_2$ [4Fe-4S]$^{1+}$ clusters exhibit two pairs of antiferromagnetically coupled iron sites corresponding (see Discussion) to one pair of ferrous ions and one with mixed-valence character ($Fe^{2.5+}-Fe^{2.5+}$). The line drawn above the data in Figure 7C is a theoretical spectrum generated with the parameters that fit the ferrous pair of the [4Fe-4S]$^{1+}$ cluster of *B. stearothermophilus* ferredoxin (*24*). The line drawn through the data in Figure 7C is a theoretical spectrum obtained by adding the contribution of the diferrous and mixed-valence pairs of the cluster of *B. stearothermophilus* ferredoxin which differs, mainly in resolution, from the spectral shape of the reduced cluster of CvFd. While the resolution of the Mössbauer spectra associated with the $S = {}^1/_2$ species is quite poor, there is no evidence that this species represents a structure other than a [4Fe-4S]$^{1+}$ cluster.

NMR Studies. To further explore the unusual properties of CvFd and to assign them to the structurally characterized clusters of the protein, NMR investigations have been carried out. In the 22−85 ppm region of all ^{1}H NMR spectra of dithionite-reduced CvFd and derivatives the number of peaks, their widths and temperature dependencies are nearly the

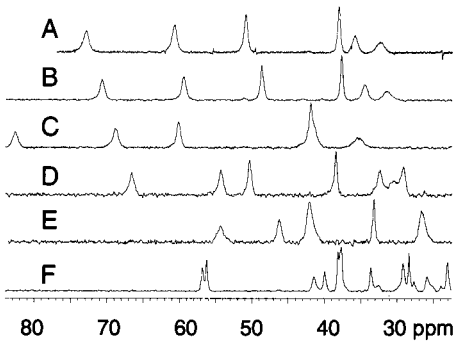

FIGURE 8: Low-field 500 MHz ^{1}H NMR spectra of dithionite-reduced 2[4Fe-4S] ferredoxins: (A) native, (B) V13G, (C) K74−, (D) Δ1K74−, (E) Δ1 CvFd, and (F) *C. acidurici* Fd. The spectra were recorded at 298 K. Assignments for native and V13G CvFd are given in Tables 1 and 2, respectively.

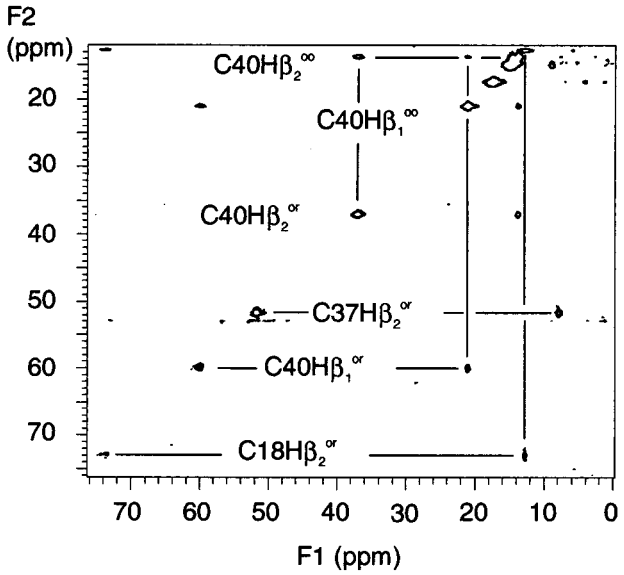

FIGURE 9: Low-field EXSY spectrum of dithionite-reduced C57S CvFd. The spectrum was recorded in D_2O at 293 K with a mixing time of 5 ms and a repetition time of 60 ms. Two hundred fifty-six complex t_1 increments were implemented with 288 transients per increment for a total acquisition time of 3 h. The signals at 34 ppm and of Cys-37H$\beta_1^{(or)}$ at 36.1 ppm [with its cross-correlation Cys-37H$\beta_1^{(oo)}$] are not visible at this intensity level.

same (Figure 8). The spectra of reduced CvFd could not be assigned through EXSY experiments in a mixture of oxidized and reduced proteins (*8*), most probably because the electron transfer between these molecules was too slow on the NMR time scale. This limitation has now been overcome with C57S (Figure 9) and V13G CvFd, for which EXSY correlations in mixtures of as-isolated and dithionite-reduced samples have been detected. Consequently, for these dithionite-reduced samples, $\delta > 22$ ppm signals could be assigned to protons belonging to ligands Cys-40, Cys-37, and Cys-18 of cluster II (Figure 9 and Table 1). This result agrees with the number of hyperfine-shifted signals in spectra of CvFd and derivatives ($\delta > 22$ ppm in Figure 8A−E**)** which is approximately half of that detected in spectra of reduced isopotential 2[4Fe-4S] Fd (Figure 8F; *9*) since only low-field shifted β-protons close to cluster II are observed in CvFd. Moreover, the low-field ^{1}H NMR spectra of V13G (Figure 8B), C57S (Figure 9), and of D12G and Y30F CvFd (not shown), all variants with amino acid substitutions close to cluster I, are nearly identical to that of CvFd, indicating

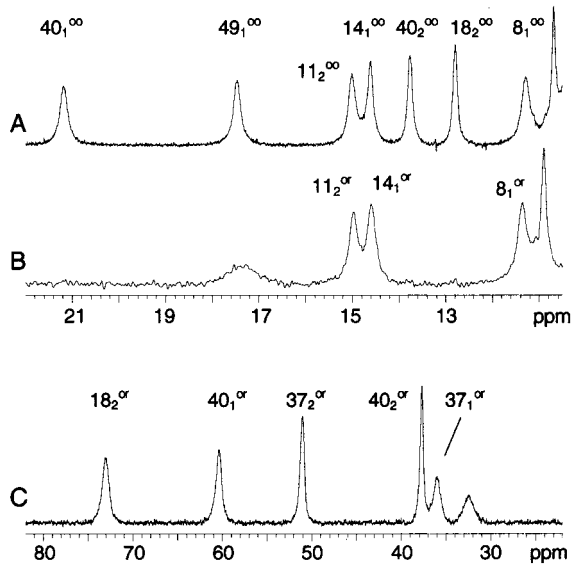

FIGURE 10: Comparison of the ^{1}H NMR spectra of C57S CvFd: (A) oxidized protein, (B) same spectral range for the dithionite-reduced protein, and (C) very low-field part of the spectrum shown in panel B. The spectra were recorded at 298 K. Assignments are from Table 1.

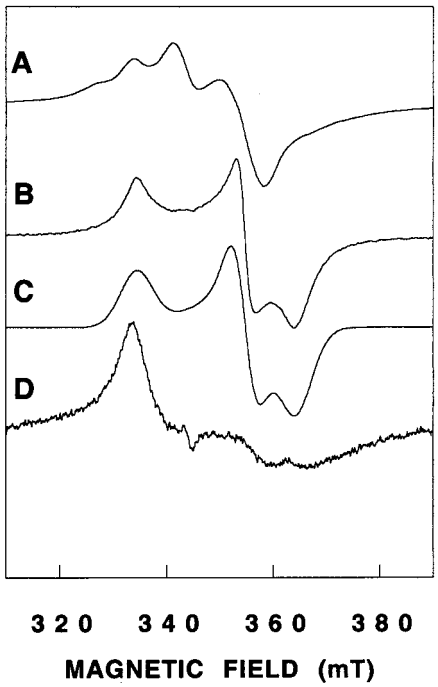

FIGURE 11: X-band EPR spectra of V13G CvFd. (A) Reduced protein at 7.5 K. (B) Reduced protein at 30 K. (C) Numerical simulation of the spectrum in panel B obtained with the following parameters: $g_{X,Y,Z} = 1.891, 1.944, 2.063$, $\sigma_{X,Y,Z} = 0.024, 0.010, 0.011$, Euler angles between tensors $\mathbf{g_0}$ and $\mathbf{p}$ of 87°, −50°, and 67°, correlation coefficients of 1, 1, and 1. (D) Spectrum at 7.5 K of the ca. 10% reduced protein.

that the assignments obtained for dithionite-reduced C57S and V13G CvFd apply with only minor adjustments to CvFd (Table 1).

In contrast, the low-field NMR patterns of the Y44C, K74E, K74−, Δ1, and Δ1K74− CvFd variants, all of them with substitutions around cluster II, differ from that of CvFd (Figure 8). The resonances in the K74E (not shown) and K74− spectra are more shifted than in the spectrum of CvFd. On the contrary, the signals of Y44C and Δ1 CvFd are less shifted than those of CvFd. Oxidized and dithionite-reduced Δ1K74− CvFd exhibit ^{1}H NMR patterns that are between those of Δ1 and K74− CvFd (Figure 8C−E). Because of the lack of EXSY correlations in mixtures containing oxidized and dithionite-reduced molecules, direct assignments have not been obtained either for Δ1K74− CvFd or for other variants with substitutions close to cluster II.

At this stage, the NMR, Mössbauer, and EPR data are consistent with the previous conclusion that cluster II can be reduced by dithionite and that the potential of cluster I is too low to accept electrons from this reductant (*5*); i.e., dithionite only generates *(or)* from *(oo)* CvFd. This statement is sustained by the quantitative conversion of the spectrum of *(oo)* C57S CvFd into a completely new set of resonances upon dithionite reduction (Figure 10 and Table 1).

Evidence for Reduction of Cluster I in V13G CvFd

The reduction potential of cluster I in V13G CvFd has been measured at −600 mV in the presence of 0.4 M NaCl, i.e., the least negative value found so far for this family of proteins (*5*). A 1:10 molar ratio of dithionite to V13G CvFd generated a rapidly relaxing EPR signal (Figure 11D), similar to that exhibited by dithionite-reduced cluster II of CvFd (Figure 6). Further reduction of V13G CvFd in the presence of DMTQ and 0.4 M NaCl resulted in a complex EPR spectrum, notably different from those of other CvFd derivatives (Figure 11A). Double integration of the signal of Figure 11A yielded 1.7 spins/molecule for V13G CvFd, a value substantially larger than those obtained for other CvFd derivatives (1 spin/molecule; see above), suggesting that cluster I in this variant can be reduced by dithionite at pH 8.2. Therefore, the complex features observed in the EPR spectrum of V13G CvFd (Figure 11A) must be attributed to magnetic interactions between the two $S = {}^1/_2$ clusters, as observed with fully reduced isopotential 2[4Fe-4S] proteins (*23*, *25*). At higher temperatures, the EPR spectra exhibit an interesting behavior; above ca. 20 K, the complex signal of the interacting $S = {}^1/_2$ clusters changes into a rhombic, slow relaxing signal at $g = 2.064, 1.943$, and 1.893 (Figure 11B). This spectral change is due to the shortening of the cluster II relaxation time which singles out the signal contributed by cluster I above 20 K. This slowly relaxing rhombic signal accounts for ca. 0.8 spin/molecule, and its shape (Figure 11B) is quite different from that of the cluster II signal detected in partly reduced V13G CvFd (Figure 11D).

The low-field part of the NMR spectrum of dithionite-reduced V13G CvFd at pH 8.2 with 0.4 M NaCl showed a unique pattern of hyperfine-shifted signals (Figure 12C). The lines with relatively low intensities have been assigned by EXSY experiments carried out with samples containing V13G CvFd molecules at different redox levels (Figure 12 and Table 2). The smaller intensity of the newly detected signals implies that they originated from a subpopulation, comprising ca. 30%, of V13G CvFd molecules in Figure 12. Upon slow reoxidation of the sample in the NMR tube, these signals disappeared and only a pattern very similar to that exhibited by the other CvFd derivatives remained (Figure 12B). In this experiment, the variations of the intensities of the NMR peaks correlated with the initial extensive reduction of the protein by dithionite that generated a mixture of *(rr)* (giving the low-intensity signals) and semireduced states. All

Table 2: Assignments of β-Cysteinyl Protons of V13G CvFd at All Accessible Redox Levels[a]

	cluster I								cluster II							
	Cys-8		Cys-11		Cys-14		Cys-53		Cys-37		Cys-40		Cys-49		Cys-18	
V13G	Hβ_1	Hβ_2	Hβ_1	Hβ_2	Hβ_1	Hβ_2	Hβ_1	Hβ_2	Hβ_1	Hβ_2	Hβ_1	Hβ_2	Hβ_1	Hβ_2	Hβ_1	Hβ_2
(rr) δ (ppm)	35.8	51.2	21.1	21.6	43.0			16.6		51.3	63.4	40.4				74.8
(rr) ΔT	C	C	AC	AC	C			AC		C	AC	AC				AC
(*) δ (ppm)	12.2	10.2	10.2	12.8	14.4	5.5	9.0	11.0	34.6	48.8	59.5	37.8				70.7
(*) ΔT	–	–	–	–	–	–	–	–	C	C	AC	AC				AC
(oo) δ (ppm)	11.8	9.7	10.0	13.0	13.7	5.4	9.2	10.7	10.5	8.0	21.1	13.7	17.5	4.3	5.9	12.7

[a] Chemical shifts (δ) were measured at 298 K. The abbreviations have the same meaning as in Table 1 and the legend of Figure 12. No correlations could be observed with two signals detected at 31.5 ppm for the (*) level, which shifts only slightly, if any, at the *(rr)* level, and at 24.5 ppm for the *(rr)* level.

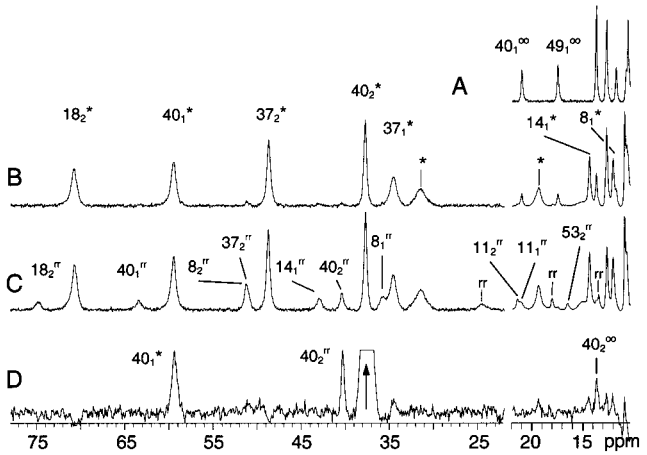

FIGURE 12: Low-field ^{1}H NMR spectra of V13G CvFd. Cys β-protons spectra, with subscripts referring to stereospecific assignments, were recorded in 20 mM potassium phosphate (pH 8.2) and 0.4 M NaCl for (A) the fully oxidized *(oo)* protein and (B and C) mixtures of different redox levels with different reducing potentials. Signals are labeled according to the redox level of the protein, *(oo)* or *(rr)*, with asterisks referring to signals specific for partially reduced samples. Part D is a selected cross section at the position of the Cys-40 Hβ_2 (37.8 ppm, arrow) of the EXSY spectrum recorded over an extended period during the reoxidation of the sample whose spectrum is shown in panel C. Except for the EXSY cross section, the intensity scale between 78 and 22 ppm is expanded 3-fold compared to that of the high-field region.

NMR signals observed upon reoxidation were related to the corresponding redox levels through cross-correlations (Figure 12 and Table 2).

DISCUSSION

Direct Assignment of the Two Redox Transitions in CvFd

The work presented here provides new insights, as revealed by NMR, EPR, and Mössbauer spectroscopy, into the properties of the two [4Fe-4S] clusters in CvFd. Two redox transitions occur in CvFd, with midpoint potentials at −460 mV (cluster II) and −660 mV (cluster I), which were previously assigned on the basis of site-directed mutagenesis and electrochemical data (*5*). The NMR studies, in particular those of V13G and C57S CvFd, unambiguously show that cluster II is more readily reduced than cluster I. The conclusion that only one of the clusters of native CvFd is reduced by dithionite is supported by EPR and Mössbauer data. Moreover, signatures of Fe−S clusters other than [4Fe-4S]$^{2+/1+}$ have not been observed in these spectroscopic studies. This agrees with the involvement of genuine [4Fe-4S]$^{2+/1+}$ clusters at all redox levels of CvFd, despite the plasticity and chemical reactivity of [4Fe-4S] in several other biological systems (*1*).

Influence of Ionizable Residues in the Vicinity of [4Fe-4S] Clusters

The chemical shifts of the β-protons belonging to Cys-11 (coordinating low potential cluster I) are pH-dependent in CvFd. This is not an unprecedented observation for Fe−S proteins. For instance, the chemical shifts of the cysteinyl protons, including those of the Cys-43 ligand, of *C. vinosum* high potential ferredoxin are sensitive to the protonation state of His-42 (*26*). In several [3Fe-4S][4Fe-4S] ferredoxins, the resonances of the cysteinyl protons close to the [3Fe-4S] cluster are pH-dependent, with a pK_a of around 5.5 (*27*, *28*). The involvement of the Asp-15 carboxylate has been demonstrated in the case of *Azotobacter vinelandii* FdI (*29*). Since the sensitivity of the NMR signals to pH disappears in D12G CvFd (Figure 5), the carboxylate group of Asp-12 is responsible for the effect. It is noteworthy that the measured pK_a of 6.3 is ca. 2 pH units higher than that of a typical solvent-exposed carboxylate (Figure 1).

The presence of carboxylate groups appears to downshift the reduction potentials of the [3Fe-4S]$^{+/0}$ center in *A. vinelandii* FdI (*29*) and of cluster I in CvFd (*5*), albeit by only 20−30 mV. Furthermore, in *A. vinelandii* FdI, Asp-15 has been suggested to enhance proton transfer to the [3Fe-4S]$^{+/0}$ cluster and to "gate" electron transfer (*30*, and references cited therein). A similar effect is not likely to occur in CvFd because a [4Fe-4S]$^{2+/1+}$ cluster bearing only μ_3-sulfides is less amenable to protonation than a [3Fe-4S]$^{+/0}$ cluster containing μ_2- and μ_3-sulfides. Moreover, the electrode kinetics of CvFd cluster I above pH 7 is not affected by removal of the carboxylate group of Asp-12 (*5*).

Electron Transfer in CvFd

EXSY correlations were obtained for mixture of oxidized and dithionite-reduced C57S CvFd (Figure 9) and V13G CvFd (Figure 12D). Under identical conditions, no such correlations were detected for CvFd and most of its other variants. The exchange process giving rise to cross-correlations in these experiments probably involves the viologens used as redox mediators, because no EXSY spectra have been obtained in their absence. Accordingly, the EXSY cross-correlations must build up through intermolecular exchange, as they relate resonances of molecules with a one-electron charge difference. Since steady-state NMR spectra of dithionite-reduced samples (Figures 8−10) demonstrate reduction of cluster II (Table 1), it would seem reasonable to look for

an interacting site in its vicinity. No exchange spectra were obtained for Δ1, K74E, K74−, and Δ1K74− CvFd, whereas, after modification of the environment of cluster I (as in C57S and V13G CvFd, Figure 1), EXSY cross-correlations did build up. This indicates that structural changes around cluster I are required to increase the overall rate of electron transfer, involving the electron originating from cluster II, between the clusters of CvFd and the redox mediators.

The occurrence of two redox transitions differing by ca. 200 mV in CvFd readily explains why the NMR spectra of the protein (ref *8* and this work) differ from those of several isopotential 2[4Fe-4S] ferredoxins (*9*). In the latter, the rate of fast electron exchange between the two clusters that has been estimated to be 5×10^6 s^{-1} on average (*9)* contributes to the widths of the Cys β-proton signals specifically assigned to the partially reduced [*(or)* and *(ro)*] proteins. The signals arising from all partially reduced CvFd proteins do not exhibit the same broadening effect (Figures 8−10 and 12). The time resolution of the NMR measurements at 500 MHz is thus not suitable for estimating any electron transfer rates which may occur in CvFd and derivatives.

No resonances corrresponding to fully reduced proteins were detected in the studied samples, except for V13G CvFd. Moreover, the spectra of the partially reduced proteins show evidence for strongly shifted resonances associated with protons close to cluster II and weakly, positively or negatively, shifted resonances associated with protons close to cluster I compared to their locations in spectra of oxidized proteins (Figures 9 and 10). These results agree with the selective reduction of cluster II in all these samples in generating *(or)*.

For V13G CvFd, a subset of signals, labeled *(rr)* in Figure 12, is readily associated with the fully (two electrons) reduced protein. These resonances display EXSYcorrelations with signals of the partially reduced sample, labeled with an asterisk in Figure 12, which give a pattern very similar to those of spectra of other dithionite-reduced CvFd derivatives (Figures 8−10). The labeled lines of Figure 12B may thus be interpreted as having the same origin as the most shifted signals of Figures 8−10, namely, as being the spectral signature of proteins in which the added electron is exclusively on cluster II [*(or)*]. However, the almost uniform chemical shift increments for protons close to cluster II in passing from one-electron- to two-electron-reduced V13G CvFd (Figure 12) challenge this view and suggest that the pattern of Figure 12B may result from very fast electron exchange between *(or)*, estimated to be about 95% of the molecules (*9*, *31*), and *(ro)*, about 5%. The lines are therefore expected to be exchange-narrowed as the relevant rate is the sum of the rate corresponding to the thermodynamically favorable electron jump from cluster I to cluster II and of the rate for the uphill back transfer (*32*). With the present set of samples, we have not found fully conclusive experimental evidence allowing us to decide between these two possibilities, and the topic will be the subject of further work.

Electronic Structure of [4Fe-4S]$^{1+}$ Clusters in Ferredoxins

Cluster II. Reduced cluster II of CvFd is an $S = {}^1/_2$ [4Fe-4S]$^{1+}$ cluster; no EPR signals originating from molecules with $S \geq {}^3/_2$ ground states were detected, in contrast to what is sometimes observed for other [4Fe-4S]$^{1+}$ clusters, including some coordinated by unconventional sequence motifs for ferredoxins (*33*−*35*, and references cited therein) as found for cluster II of CvFd.

However, $S = {}^3/_2$ excited states are likely low-lying in energy as indicated by the fast relaxation properties of this cluster in CvFd and derivatives. Moreover, the broad features observed by EPR most likely reflect a cluster whose exchange-coupling constants are distributed or for which low-lying spin multiplets are mixed by (distributed) zero-field splittings into the ground doublet. Either effect will give rise to distributed spin projection coefficients and thus to a dispersion of *g* values and magnetic hyperfine fields sensed by Mössbauer spectroscopy. In EPR spectra of [2Fe-2S]$^{1+}$ (*36*) and [3Fe-4S]$^{1+}$ (*37*) clusters, such effects enhanced the spin−lattice relaxation rates and led to an increase of the **g**-tensor anisotropy and to **g**-strain broadening. Although no quantitative model has yet been developed for [4Fe-4S]$^{1+}$ clusters, the correlation between the efficiency of the spin−lattice relaxation, **g**-tensor anisotropy, and **g**-strain remains qualitatively valid, as experimentally observed for center F_X of photosystem I (*38*) and for the [4Fe-4S]$^{1+}$ cluster of *Pyrococcus furiosus* ferredoxin (*39*).

For cluster II of CvFd, the partial correlation between random variables describing the **g**-strain broadening might reveal several independent structural contributions to the **g**-strain effect. Indeed, a full correlation between the elements of the **p**-tensor has been interpreted as indicating a unique physical origin for **g**-strain, such as a uniform stress on the protein (*20*). Conversely, the partial correlation of p_i variables, as observed here for CvFd, may indicate several independent causes for the **g**-strain perhaps related to peculiar structural elements of the protein. This suggests that the two-turn loop between Cys-40 and Cys-49, which is removed in Δ1 CvFd, and the long C-terminal helix may be regarded as the structural causes of the special **g**-strain properties exhibited by dithionite-reduced cluster II.

Cluster I. In contrast to the EPR signal of cluster II, the sharper signal attributed to cluster I in V13G CvFd relaxes slowly (Figure 11B). This represents the first observation in 2[4Fe-4S]$^{1+}$ ferredoxins of the conversion of a complex signal originating from magnetic interactions between clusters into a simple rhombic signal associated with a single cluster. Similar changes with temperature of the complex EPR signal arising from interacting groups with different relaxation properties have been observed in other systems (*40*, *41*).

Electron Distribution in [4Fe-4S]$^{1+}$. Typically, the Mössbauer spectra of reduced $S = {}^1/_2$ [4Fe-4S]$^{1+}$ clusters consist of two spectral components, each representing two nearly equivalent iron sites (*16*, *24*, *42*). One component belongs to a diferrous pair; the iron sites of this pair have magnetic hyperfine tensors with positive components, implying that the pair spin $S_{12} = 4$ or 3 (*43*) is antiparallel to the cluster spin $S = {}^1/_2$. The second spectral component observed for [4Fe-4S]$^{1+}$ clusters represents a valence-delocalized $Fe^{2.5+}$−$Fe^{2.5+}$ pair, with negative magnetic hyperfine tensor components, implying that its pair spin ($S_{34} = {}^9/_2$ or ${}^7/_2$) is parallel to the cluster spin. The Mössbauer spectrum of reduced cluster II is compatible with a [4Fe-4S]$^{1+}$ cluster, but it is less resolved than that of *B. stearothermophilus* ferredoxin, which was taken as an example of a protein-bound

[4Fe-4S] reduced cluster with an $S = {}^1/_2$ ground state. The possible reasons for the differences have been discussed above.

The spin of the delocalized pair is parallel to the total spin of the ground state, and the contact shift of the bound cysteinyl β-CH_2 protons should follow a Curie-type temperature dependence. On the other hand, anti-Curie behavior is anticipated for the corresponding resonances associated with cysteinyl residues bound to the ferrous pair. Indeed, such temperature dependencies were predicted by calculating the thermally corrected terms accounting for the involvement of excited states of high potential $[4Fe\text{-}4S]^{3+}$ clusters (*43*). This rationale has been used to interpret the NMR data obtained from the $[4Fe\text{-}4S]^{1+}$ ferredoxin of *P. furiosus* (*44*). Therefore, as long as the spin coupling scheme of each cluster in CvFd is similar, the temperature dependencies of the NMR resonances directly reflect the proximity of the corresponding protons to either the ferrous or the mixed-valence pair of irons.

Cluster-bound cysteines of [4Fe-4S] ferredoxins can be labeled I−IV according to their location in the $C^{I}xxC^{II}xxC^{III}\cdot\cdot\cdot C^{IV}P$ coordinating sequence motif. For reduced cluster II of all forms of CvFd studied here, the ^1H NMR signals of Cys^{I}-37 exhibit a Curie-type behavior, while the resonances of Cys^{II}-40 and Cys^{IV}-18 protons exhibit an anti-Curie temperature dependence (no resonances belonging to Cys^{III}-49 have been assigned). The same pattern was observed for other 2[4Fe-4S] ferredoxins (*18*), for which the signals of Cys^{I} and Cys^{III} follow a Curie law and those of Cys^{II} and Cys^{IV} exhibit an anti-Curie behavior. This suggests that the insertion of the two-turn loop between Cys-40 and Cys-49 of CvFd does not lead to a migration of the $Fe^{2.5+}-Fe^{2.5+}$ pair as compared to clusters of ferredoxins that have only two residues between the equivalent ligands. A similar distribution of Curie and anti-Curie signals can be deduced for cluster I of V13G CvFd (Table 2). Interestingly, this distribution has been observed for all low potential protein-bound clusters with cysteine-only coordination examined so far (*18*, *44*, *45*). Since these proteins, in particular the ones investigated here, exhibit different properties, the differences cannot be related to different electronic distributions over the centers, as once suggested (*8*). To date, only $[4Fe\text{-}4S]^{1+}$ clusters with at least one noncysteinyl (Ser or Asp) ligand have provided different sequence-related electronic distributions (*44*).

Concluding Remarks

The spectroscopic data reported here for CvFd confirm that this protein and others of the same family (*4*−*6*) exhibit two redox transitions separated by almost 200 mV. Moreover, the NMR results provide the unambiguous assignments of these transitions to cluster I at −660 mV and to cluster II at −460 mV for CvFd. This conclusion is in agreement with that obtained from shifts of the reduction potentials associated with site specific amino acid replacements (*5*). The data presented here also show that the failure of reducing cluster I with dithionite is not due to some very slow reaction, but rather to the low potential of this cluster.

Despite these significant differences with respect to other low potential [4Fe-4S] clusters in ferredoxins, the temperature dependence pattern of the cysteinyl ^1H NMR signals of both CvFd clusters (Tables 1 and 2) is strikingly similar to that observed for other all-cysteine coordinated $[4Fe\text{-}4S]^{1+}$ clusters in proteins (*18*, *44*, *45*). The observed location of the mixed-valence pair in such clusters seems to be insensitive to many geometrical differences around the clusters, including the conformation of cysteine ligands as seen here for cluster II of CvFd. This conclusion is in contrast with the behavior of $[4Fe\text{-}4S]^{3+}$ clusters of high potential ferredoxins for which the geometric distribution of the mixed-valence pair varies between different proteins (*46*). Moreover, the detailed and potentially predictive correlations between the electronic structure of $[4Fe\text{-}4S]^{2+/1+}$ clusters and their macroscopic properties in proteins, such as the value of the reduction potential, the conformation of the ligands, or the electron transfer rates, remain elusive despite promising theoretical attempts (*47*, *48*). Further work along these lines is clearly needed for a full appreciation of the functional consequences of the mutual interactions between [4Fe-4S] clusters and their protein environment.

SUPPORTING INFORMATION AVAILABLE

A table with ^1H and backbone ^{13}C and ^{15}N resonance assignments of oxidized CvFd. This material is available free of charge via the Internet at http://pubs.acs.org.

REFERENCES

1. Beinert, H., Holm, R. H., and Münck, E. (1997) *Science 277*, 653−659.
2. Dauter, Z., Wilson, K. S., Sieker, L. C., Meyer, J., and Moulis, J.-M. (1997) *Biochemistry 36*, 16065−16073.
3. Lauble, H., and Stout, C. D. (1995) *Proteins: Struct., Funct., Genet. 22*, 1−11.
4. Moulis, J.-M. (1996) *Biochim. Biophys. Acta 1308*, 12−14.
5. Kyritsis, P., Hatzfeld, O. M., Link, T. A., and Moulis, J.-M. (1998) *J. Biol. Chem. 273*, 15404−15411.
6. Gao-Sheridan, H. S., Pershad, H. R., Armstrong, F. A., and Burgess, B. K. (1998) *J. Biol. Chem. 273*, 5514−5519.
7. Moulis, J.-M., and Davasse, V. (1995) *Biochemistry 34*, 16781−16788.
8. Huber, J. G., Gaillard, J., and Moulis, J.-M. (1995) *Biochemistry 34*, 194−205.
9. Kyritsis, P., Huber, J. G., Quinkal, I., Gaillard, J., and Moulis, J.-M. (1997) *Biochemistry 36*, 7839−7846.
10. Mayhew, S. G. (1978) *Eur. J. Biochem. 85*, 535−547.
11. Moulis, J.-M., Sieker, L. C., Wilson, K. S., and Dauter, Z. (1996) *Protein Sci. 5*, 1765−1775.
12. Quinkal, I., Davasse, V., Gaillard, J., and Moulis, J.-M. (1994) *Protein Eng. 7*, 681−687.
13. Hagen, W. R., Hearshen, D. O., Sands, R. H., and Dunham, W. R. (1985) *J. Magn. Reson. 61*, 220−232.
14. Bertrand, P., Camensuli, P., More, C., and Guigliarelli, B. (1996) *J. Am. Chem. Soc. 118*, 1426−1434.
15. Moulis, J.-M., Auric, P., Gaillard, J., and Meyer, J. (1984) *J. Biol. Chem. 259*, 11396−11402.
16. Christner, J. A., Janick, P. A., Siegel, L. M., and Münck, E. (1983) *J. Biol. Chem. 258*, 11157−11164.
17. Mullinger, R. N., Cammack, R., Rao, K. K., Hall, D. O., Dickson, D. P. E., Johnson, C. E., Rush, J. D., and Simopoulos, A. (1975) *Biochem. J. 151*, 75−83.
18. Bertini, I., Capozzi, F., Luchinat, C., Piccioli, M., and Vila, A. J. (1994) *J. Am. Chem. Soc. 116*, 651−660.
19. Perkins, S. J., and Wüthrich, K. (1979) *Biochim. Biophys. Acta 576*, 409−423.
20. Hagen, W. R. (1992) *Adv. Inorg. Chem. 38*, 165−222.
21. Guigliarelli, B., Asso, M., More, C., Augier, V., Blasco, F., Pommier, J., Giordano, G., and Bertrand, P. (1992) *Eur. J. Biochem. 207*, 61−68.

22. Guigliarelli, B., Guillaussier, J., More, C., Setif, P., Bottin, H., and Bertrand, P. (1993) *J. Biol. Chem. 268*, 900−908.
23. More, C., Camensuli, P., Dole, F., Guigliarelli, B., Asso, M., Fournel, A., and Bertrand, P. (1996) *J. Biol. Inorg. Chem. 1*, 152−161.
24. Middleton, P., Dickson, D. P. E., Johnson, C. E., and Rush, J. D. (1978) *Eur. J. Biochem. 88*, 135−141.
25. Mathews, R., Charlton, S., Sands, R. H., and Palmer, G. (1974) *J. Biol. Chem. 249*, 4326−4328.
26. Nettesheim, D. G., Meyer, T. E., Feinberg, B. A., and Otvos, J. D. (1983) *J. Biol. Chem. 258*, 8235−8239.
27. Cheng, H., Grohmann, K., and Sweeney, W. (1990) *J. Biol. Chem. 265*, 12388−12392.
28. Gorst, C. M., Yeh, Y.-H., Teng, Q., Calzolai, L., Zhou, Z.-H., Adams, M. W. W., and La Mar, G. N. (1995) *Biochemistry 34*, 600−610.
29. Shen, B., Jollie, D. R., Stout, C. D., Diller, T. C., Armstrong, F. A., Gorst, C. M., La Mar, G. N., Stephens, P. J., and Burgess, B. K. (1994) *J. Biol. Chem. 269*, 8564−8575.
30. Hirst, J., Duff, J. L. C., Jameson, G. N. L., Kemper, M. A., Burgess, B. K., and Armstrong, F. A. (1998) *J. Am. Chem. Soc. 120*, 7085−7094.
31. Turner, D. L., Salgueiro, C. A., Catarino, T., LeGall, J., and Xavier, A. V. (1996) *Eur. J. Biochem. 241*, 723−731.
32. Gaillard, J., Zhuang-Jackson, H., and Moulis, J.-M. (1996) *Eur. J. Biochem. 238*, 346−349.
33. Duin, E. C., Lafferty, M. E., Crouse, B. R., Allen, R. M., Sanyal, I., Flint, D. E., and Johnson, M. K. (1997) *Biochemistry 36*, 11811−11820.
34. Arendsen, A. F., Hadden, J., Card, G., McAlpine, A. S., Bailey, S., Zaitsev, V., Duke, E. H. M., Lindley, P. F., Kröckel, M., Trautwein, A. X., Feiters, M. C., Charnok, J. M., Garner, C. D., Marritt, S. J., Thomson, A. J., Kooter, I. M., Johnson, M. K., Van den Berg, W. A. M., Van Dongen, W. M. A. M., and Hagen, W. R. (1998) *J. Biol. Inorg. Chem. 3*, 81−95.
35. Telser, J., Huang, H., Lee, H.-I., Adams, M. W. W., and Hoffman, B. M. (1998) *J. Am. Chem. Soc. 120*, 861−870.
36. Bertrand, P., Guigliarelli, B., and More, C. (1991) *New J. Chem. 15*, 445−454.
37. Guigliarelli, B., More, C., Bertrand, P., and Gayda, J.-P. (1986) *J. Chem. Phys. 85*, 2774−2778.
38. Bertrand, P., Guigliarelli, B., Gayda, J.-P., Setif, P., and Mathis, P. (1988) *Biochim. Biophys. Acta 933*, 393−397.
39. Conover, R. C., Kowal, A. T., Fu, W., Park, S., Aono, S., Adams, M. W. W., and Johnson, M. K. (1990) *J. Biol. Chem. 265*, 8533−8541.
40. Fielding, L., More, K. M., Eaton, G. R., and Eaton, S. S. (1986) *J. Am. Chem. Soc. 108*, 8194−8196.
41. Guigliarelli, B., More, C., Fournel, A., Asso, M., Hatchikian, E. C., Williams, R., Cammack, R., and Bertrand, P. (1995) *Biochemistry 34*, 4781−4790.
42. Münck, E., Papaefthymiou, V., Surerus, K. K., and Girerd, J.-J. (1988) in *Metal Clusters in Proteins* (Que, L., Jr., Ed.) pp 302−325, American Chemical Society, Washington, DC.
43. Noodleman, L., Chen, J.-L., Case, D. A., Giori, C., Rius, G., Mouesca, J.-M., and Lamotte, B. (1995) in *Nuclear Magnetic Resonance of Paramagnetic Macromolecules* (La Mar, G. N., Ed.) pp 339−367, NATO ASI Series, Kluwer Academic Publishers, Dordrecht, The Netherlands.
44. Calzolai, L., Gorst, C. M., Bren, K. L., Zhou, Z.-H., Adams, M. W. W., and La Mar, G. N. (1997) *J. Am. Chem. Soc. 119*, 9341−9350.
45. Lebrun, E., Simenel, C., Guerlesquin, F., and Delepierre, M. (1996) *Magn. Res. Chem. 34*, 873−880.
46. Bertini, I., Capozzi, F., Eltis, L. D., Felli, I. C., Luchinat, C., and Piccioli, M. (1995) *Inorg. Chem. 34*, 2516−2523.
47. Mouesca, J.-M., Chen, J. L., Noodleman, L., Bashford, D., and Case, D. A. (1994) *J. Am. Chem. Soc. 116*, 11898−11914.
48. Bominaar, E. L., Achim, C., Borshch, S. A., Girerd, J.-J., and Münck, E. (1997) *Inorg. Chem. 36*, 3689−3701.

BI982894U